Nucleotide- and Protein-Dependent Functions of *Actg1*

Lauren J. Sundby[a], William M. Southern[b], Katelin M. Hawbaker[c], Jesús M. Trujillo[b], Benjamin J. Perrin[c], and James M. Ervasti[b,*]

[a]Program in Molecular, Cellular, Developmental Biology, and Genetics, and [b]Department of Biochemistry, Molecular Biology, and Biophysics, University of Minnesota, Minneapolis, MN 55455; [c]Department of Biology, Indiana University-Purdue University Indianapolis, Indianapolis, IN 46022

ABSTRACT **Cytoplasmic β- and γ-actin proteins are 99% identical but support unique organismal functions. The cytoplasmic actin nucleotide sequences *Actb* and *Actg1*, respectively, are more divergent but still 89% similar. *Actb*$^{-/-}$ mice are embryonic lethal and *Actb*$^{-/-}$ cells fail to proliferate, but editing the *Actb* gene to express γ-actin (*Actb*$^{c-g}$) resulted in none of the overt phenotypes of the knockout revealing protein-independent functions for *Actb*. To determine if *Actg1* has a protein-independent function, we crossed *Actb*$^{c-g}$ and *Actg1*$^{-/-}$ mice to generate the bG/0 line, where the only cytoplasmic actin expressed is γ-actin from *Actb*$^{c-g}$. The bG/0 mice were viable but showed a survival defect despite expressing γ-actin protein at levels no different from bG/gG with normal survival. A unique myopathy phenotype was also observed in bG/0 mice. We conclude that impaired survival and myopathy in bG/0 mice are due to loss of *Actg1* nucleotide-dependent function(s). On the other hand, the bG/0 genotype rescued functions impaired by *Actg1*$^{-/-}$, including cell proliferation and auditory function, suggesting a role for γ-actin protein in both fibroblasts and hearing. Together, these results identify nucleotide-dependent functions for *Actg1* while implicating γ-actin protein in more cell-/tissue-specific functions.**

Monitoring Editor
Thomas Pollard
Yale University

Received: Feb 25, 2022
Revised: May 10, 2022
Accepted: May 11, 2022

INTRODUCTION

Actin is an essential cellular protein involved in many important functions including cell motility, cytokinesis, muscle contraction, structural support, and regulation of gene expression (Pollard and Cooper, 2009). In mammals, these functions are carried out by the actin family of proteins, which is composed of the four muscle-specific actins, α-skeletal, α-smooth, α-cardiac, and γ-smooth, and the two ubiquitously expressed cytoplasmic actins, β- and γ-actin, each expressed from a unique gene. As a key component of many essential cellular processes, it is unsurprising that mutations in either cytoplasmic actin gene are associated with severe developmental defects in humans, and as β- and γ-actin are also important constituents of the stereocilia in the inner ear, mutations also often lead to different kinds of syndromic and nonsyndromic deafness (Zhu *et al.*, 2003; Rivière *et al.*, 2012; Rubenstein & Wen, 2014; Latham *et al.*, 2018; Miyajima *et al.*, 2020).

While all six mammalian actins are highly similar, the cytoplasmic actins share 99% sequence identity, differing by only 4 of 375 amino acids. The cytoplasmic actin gene sequences, *Actb* and *Actg1*, are highly conserved and also very similar, sharing 89% of their coding sequences in mice (Perrin and Ervasti, 2010). However, despite the high sequence similarity, the cytoplasmic actins seem to occupy unique biological niches, as demonstrated by the distinct differences in their respective gene knockout models. *Actb*$^{-/-}$ mice are embryonic lethal, with all embryos dying by E8.5 (Shawlot *et al.*, 1998; Shmerling *et al.*, 2005; Bunnell *et al.*, 2011) while *Actg1*$^{-/-}$ mice are viable with increased perinatal lethality (Belyantseva *et al.*, 2009). *Actb*$^{-/-}$ mouse embryonic fibroblasts (MEFs) also failed to proliferate and had significantly impaired cell migration (Bunnell *et al.*, 2011), while *Actg1*$^{-/-}$ MEFs presented with a small, but significant, decrease in proliferation and normal motility (Bunnell and Ervasti, 2010).

This article was published online ahead of print in MBoC in Press (http://www.molbiolcell.org/cgi/doi/10.1091/mbc.E22-02-0054) on May 20, 2022.

*Address correspondence to: James Ervasti (jervasti@umn.edu).

Abbreviations used: α_{sm}-actin, α smooth-muscle actin; ABR, auditory brainstem response; *Actb*$^{c-g}$, *Actb* coding γ-actin; F-actin, filamentous actin; G-actin, globular actin; MEF, mouse embryonic fibroblast; OHC, outer hair cell; SRF, serum response factor.

The specific mechanisms by which nearly identical β- and γ-actin function differently remain an outstanding question. Current data suggest that functional differences between them may be due to isoform specific interactions with actin-associated proteins, distinct patterns of posttranslational modifications, or variations in mRNA abundance and localization (reviewed in Kashina, 2020). At the protein level, a number of studies have reported isoform-specific interactions with different actin-binding proteins. β-Actin has shown preferential binding to myosin 2B, tropomyosin (Pathan-Chhatbar *et al.*, 2018), myosin 2C1 (Müller *et al.*, 2013), betacap73 (Shuster *et al.*, 1996; Welch *et al.*, 2005), and DIAPH3 (Chen *et al.*, 2017), while γ-actin shows preference for myosin 7a (Müller *et al.*, 2013). Between the two cytoplasmic actins, studies have shown that only β-actin undergoes N-terminal arginylation (Karakozova *et al.*, 2006; Kashina, 2006; Saha *et al.*, 2010; Pavlyk *et al.*, 2018); however, a new study suggests that N-terminal arginylation of β-actin is nominal in the presence of very high rates of N-terminal acetylation (Drazic *et al.*, 2021). β- and γ-actin have also shown unique cellular distribution in different tissues and during different cell stages, with β-actin localizing to the cleavage furrow and γ-actin to the cell cortex during cell division (Otey *et al.*, 1986, 1988; Dugina *et al.*, 2009; Chen *et al.*, 2017). The *Actb* mRNA contains a unique "zipcode" sequence in the 3′ UTR that interacts with RNA localization proteins, such as Zipcode binding protein 1, to promote local translation of the β-actin protein (Kislauskis *et al.*, 1994; Ross *et al.*, 1997; Hüttelmaier *et al.*, 2005; Pan *et al.*, 2007).

While much has been revealed about the different roles of the two cytoplasmic actins, the essential differences conferring unique impacts on organismal survival have recently been linked to the nucleotide sequence of *Actb*, rather than the β-actin amino acid sequence. We and others (Vedula *et al.*, 2017; Patrinostro *et al.*, 2018) used different gene editing technologies to generate mice that expressed γ-actin protein from *Actb,* establishing a β-actin protein specific knockout that maintains an intact *Actb* nucleotide sequence, named $Actb^{c-g}$. In direct contrast to the embryonic lethality of the $Actb^{-/-}$ (Bunnell *et al.*, 2011), the $Actb^{c-g}$ mice were largely phenotypically normal with no defect in survival (Patrinostro *et al.*, 2018; Vedula *et al.*, 2017). $Actb^{c-g}$ MEFs also had normal proliferation rates and migration patterns (Patrinostro *et al.*, 2018; Vedula *et al.*, 2017). These results demonstrated that it is not the loss of β-actin that causes embryonic lethality in $Actb^{-/-}$ mice, but rather the loss of the intact *Actb* nucleotide sequence, suggesting that *Actb* must have protein-independent functions. However, the $Actb^{c-g}$ mice also developed progressive hearing loss due to degradation of inner ear hair cell stereocilia, supporting a tissue-specific function for β-actin protein (Patrinostro *et al.*, 2018).

In this study, we assessed whether the *Actg1* nucleotide sequence also supports essential protein-independent functions by generating a novel mouse model where the only cytoplasmic actin expressed is γ-actin from $Actb^{c-g}$, named bG/0. We found that these mice are viable and express γ-actin protein levels no different from those in control littermates. However, we observed unique phenotypes that suggest that *Actg1* and γ-actin have nucleotide- and protein-dependent functions that differ from those of *Actb* or β-actin. Together, these results reveal novel insights into the differential functions of the highly similar cytoplasmic actins, and further support previous studies implicating the importance of nucleotide specific differences between *Actb* and *Actg1*.

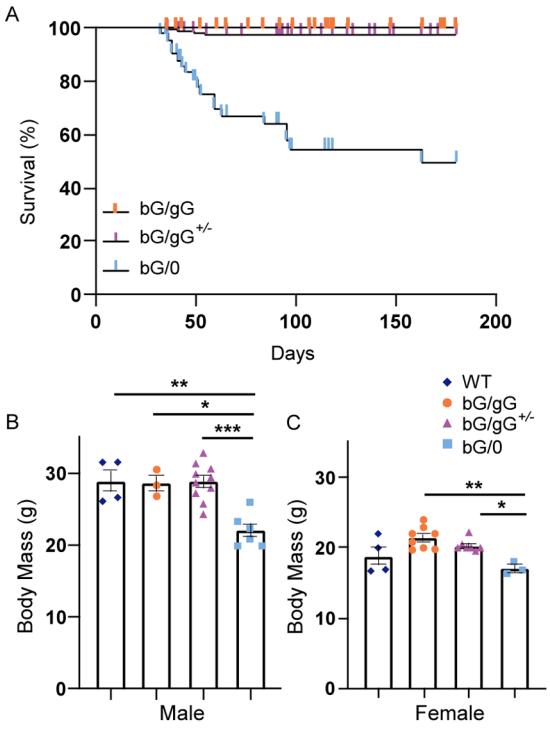

FIGURE 1: bG/0 mice are viable but are smaller and show increased post-birth mortality. (A) Kaplan-Meier survival curve of bG/gG, bG/gG$^{+/-}$, and bG/0 mice from P0 to P180 ($n \geq 34$ for each genotype). Tick marks indicate when animals were removed from the survival study before 180 d for other analyses performed in this study or animals that survived beyond the 180 d endpoint. (B, C) Body mass for male and female mice, respectively ($n \geq 3$ at 3 mo). One-way ANOVA with Bonferroni posttest was performed. *$p < 0.05$, **$p < 0.01$, ***$p < 0.001$. Error bars are SEM. Comparisons are not statistically significant unless indicated otherwise.

RESULTS

Mice expressing exclusively γ-actin from *Actb* are viable

To determine if reducing the cytoplasmic actin pool in mice to γ-actin expressed exclusively from the edited *Actb* gene supports viability, we crossed $Actb^{c-g}$ mice (Patrinostro *et al.*, 2018) with $Actg1^{+/-}$mice (Belyantseva *et al.*, 2009) to generate $Actb^{c-g/c-g}Actg1^{-/-}$ mice. Hereafter, $Actb^{c-g/c-g}Actg1^{-/-}$ mice will be referred to as bG/0, where the lowercase letter indicates the gene, the uppercase letter indicates the protein expressed, 0 indicates $Actg1^{-/-}$, and $^{+/-}$ indicates $Actg1^{+/-}$ (Supplemental Table S1). The bG/0 mice were viable but were observed in sub-Mendelian ratios at weaning: 35.02% bG/gG, 58.23% bG/gG$^{+/-}$, and only 6.75% bG/0 rather than the expected ratios of 25:50:25. bG/0 mice presented with a median survival of only 163 d, which is significantly less than bG/gG or bG/gG$^{+/-}$ littermates (Figure 1A). bG/0 mice were also significantly smaller than their bG/gG or bG/gG$^{+/-}$ littermates, and male bG/0 mice were significantly smaller than WT controls (Figure 1, B and C). Decreased survival and size of the bG/0 mice is consistent with results previously reported for $Actg1^{-/-}$ mice (Belyantseva *et al.*, 2009).

Because hypomorphic expression of cytoplasmic actins would explain the decreased viability in bG/0 mice most simply, we utilized quantitative real-time PCR (qRT-PCR) to measure isoactin transcript levels in WT, bG/gG, bG/gG$^{+/-}$, and bG/0 brain, lung, and MEF tissue. bG/0 lung and MEF total transcript levels were not significantly different from those in WT controls, while brain tissue showed a significantly increased level of total actin transcript in all bG/gG,

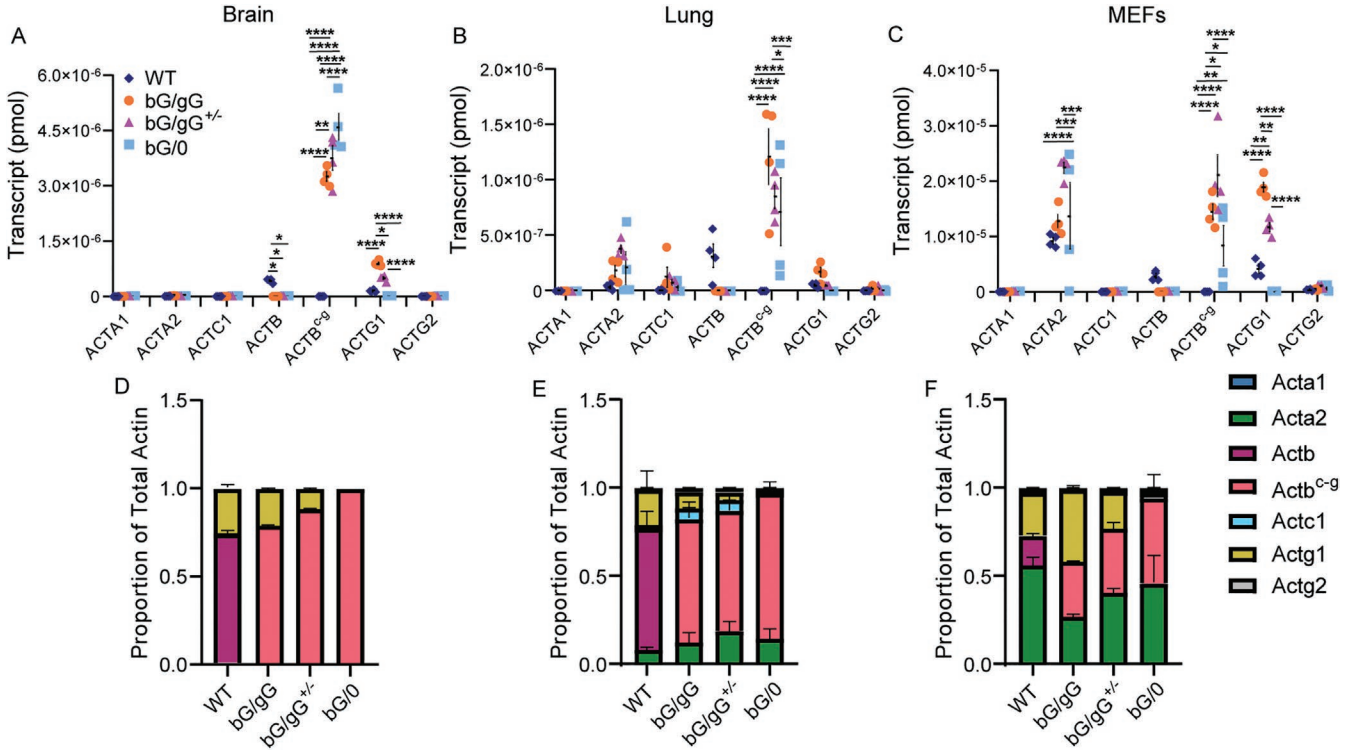

FIGURE 2: The *Actb*$^{c-g}$ transcript is upregulated with ablation of *Actg1*. (A-C) Absolute and (D-F) proportional quantification of isoactin and *Actb*$^{c-g}$ transcript in brain, lung, and MEFs of WT, bG/gG, bG/gG$^{+/-}$, and bG/0 mice and embryos ($n = 4$, in triplicate). Transcript amounts (picomoles) were calculated using a standard curve, amplified in parallel. For A-C, two-way ANOVA with Bonferroni posttest was performed. *$p < 0.05$, **$p < 0.01$, ***$p < 0.001$, ****$p < 0.0001$. Error bars are SEM. Comparisons are not statistically significant unless otherwise indicated.

bG/gG$^{+/-}$, and bG/0 samples (Supplemental Figure S1). Upon loss of intact *Actg1* in bG/0 mice, the tissues showed loss of expression of the *Actg1* transcript and a corresponding increase in expression of the *Actb*$^{c-g}$ transcript. bG/0 lungs also showed a nonsignificant increase in *Acta2* expression while MEFs showed a significant increase in *Acta2* (Figure 2, A–F). These data suggest that the bG/0 tissues compensate for loss of *Actg1* by up-regulating expression of other actin isoforms, including the edited *Actb*$^{c-g}$ allele.

We also measured relative protein levels of cytoplasmic, α_{sm}-, and total actin using quantitative Western blotting of WT, bG/gG, bG/gG$^{+/-}$, and bG/0 brain, lung, and MEF tissue. Similar to the measured transcript levels, cytoplasmic actin protein levels appeared to undergo compensatory up-regulation to maintain a WT level of total actin protein. Despite the loss of *Actg1*, we measured γ-actin protein levels that remain constant across bG/gG, bG/gG$^{+/-}$, and bG/0 mice (Figure 3, A–F), demonstrating that the *Actb*$^{c-g}$ allele is able to compensate for loss of endogenous γ-actin expressed from *Actg1*. Because we measured constant levels of γ-actin between bG/gG and bG/0 and only bG/0 presents with decreased survival, we conclude that the survival defect observed in the bG/0 mice is due to loss of the intact *Actg1* nucleotide sequence and not to the loss of γ-actin protein expression.

bG/0 MEFs appear phenotypically normal

Actb$^{-/-}$ MEFs show significant defects in proliferation and motility not observed in gene-edited *Actb*$^{c-g}$ MEFs (Bunnell and Ervasti, 2010; Bunnell *et al.*, 2011; Patrinostro *et al.*, 2017, 2018; Vedula *et al.*, 2017). Previously generated *Actg1*$^{-/-}$ MEFs also have significantly impaired proliferation (Bunnell & Ervasti, 2010), so to determine if this phenotype is caused by a loss of *Actg1*, we assessed bG/0 MEF morphology and function. Immunostained bG/0 MEFs showed γ-actin localization throughout the entirety of the cell, from the cell body to the periphery, similar to WT and bG/gG cells and present with no significant morphological differences (Figure 4A; Supplemental Figure S2, A–C). Phalloidin staining showed no overt changes in actin filaments in Figure 4B. The measured proliferation rate of bG/0 MEFs was not different from WT and bG/gG controls (Figure 4C). MEFs have the capacity to differentiate into myofibroblasts in response to a number of environmental stimuli. During this transition, cytoplasmic actin polymerizes into stress fibers and cells up-regulate expression of α_{sm}-actin (Tomasek *et al.*, 2002; Hinz, 2007; Davis and Molkentin, 2014). We have previously observed myofibroblast-like phenotypes in *Actb*$^{-/-}$, *Actg1*$^{-/-}$, and *Actb*$^{-/-}$/*Actg1*$^{-/-}$ MEFs (Patrinostro *et al.*, 2017). Despite unchanged levels of α_{sm}-actin (Figure 3C), we quantified stress fiber numbers and thickness in phalloidin-stained cells to determine if there might be other myofibroblast-like phenotypes in bG/0 MEFs. In bG/0 MEFs, no change in fiber thickness or number was observed from those in WT and bG/gG controls (Figure 4, D–F). Together, these results suggest that it is the loss of γ-actin and not the *Actg1* nucleotide sequence that causes MEFs to undergo a fibroblast-to-myofibroblast transition

The polymerization state of actin in cells is an important regulator of cell function and elicits changes through shifting the ratio of polymerized F-actin to monomeric G-actin (reviewed in Kashina, 2020). Previous studies have shown that loss of *Actb*, but not β-actin or *Actg1*, causes a significant decrease in G-actin (Bunnell and Ervasti, 2010; Bunnell *et al.*, 2011; Patrinostro *et al.*, 2018). In bG/0 MEFs, we observed an insignificant decrease in the G- to F-actin ratio of γ- and α_{sm}-actin and a significant decrease in the amount of

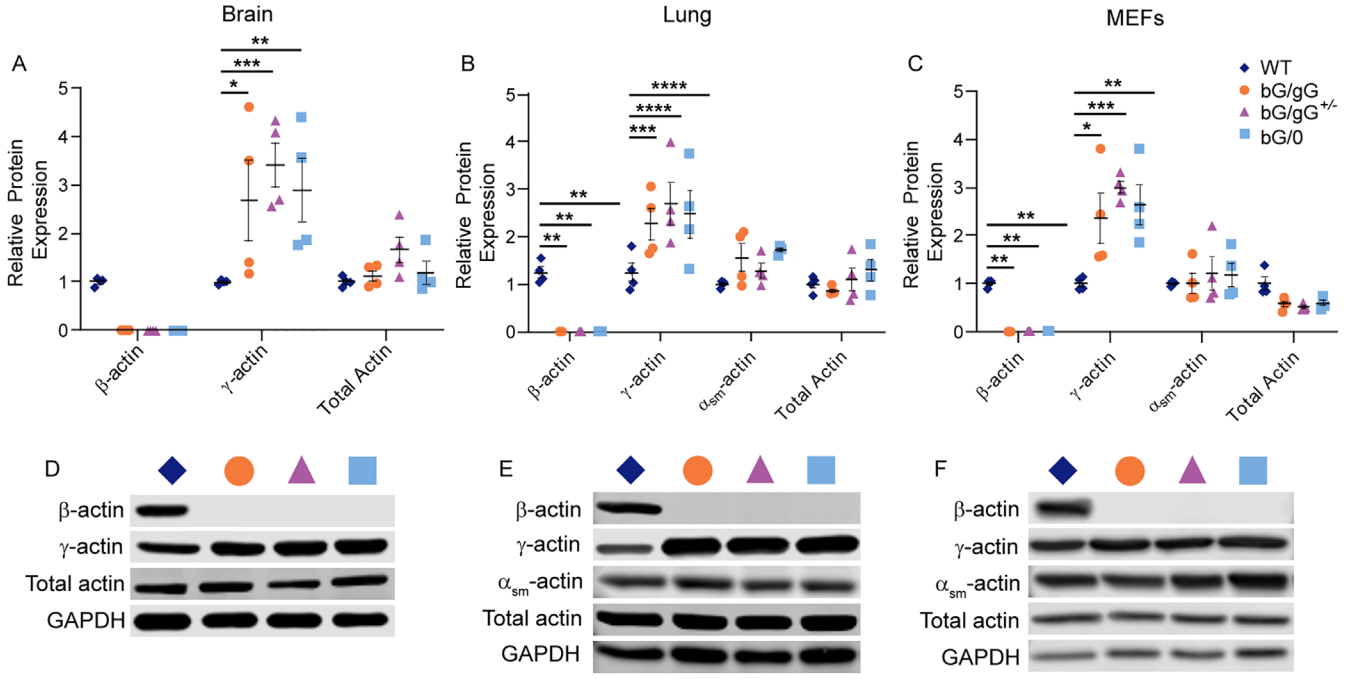

FIGURE 3: Mice expressing γ-actin from *Actb*$^{c-g}$ maintain WT levels of total actin protein. (A-C) Relative actin isoform protein expression in WT, bG/gG, bG/gG$^{+/-}$, and bG/0 brain, lungs, and MEFs ($n = 4$). *x*-axis denotes actin isoform and *y*-axis denotes relative protein expression normalized to GAPDH and relative to WT. (D-F) Representative Western blots of brain, lung, and MEFs. Two-way ANOVA with Bonferroni posttest was performed. *$p < 0.05$, **$p < 0.01$, ***$p < 0.001$, ****$p < 0.0001$. Error bars are SEM. Comparisons are not statistically significant unless otherwise indicated.

G-actin for total actin from those in WT and bG/gG controls (Figure 4G). The significance of the G-actin decrease for total actin is likely due to the combined insignificant decrease observed for both γ- and α_{sm}-actin.

One of the key signaling pathways that responds to changes in the polymerization state of actin is the serum response factor (SRF)/myocardin-related transcription factor (MRTF) signaling pathway (Vartiainen *et al.*, 2007; Olson and Nordheim, 2010; Baarlink *et al.*, 2013; Esnault *et al.*, 2014). Quantitative Western blotting revealed no change in SRF or MRTF-A expression in bG/0 MEFs from WT, bG/gG, and bG/gG$^{+/-}$ (Figure 4H). Changes in cellular F-actin also impacts the Hippo signaling pathway through central effectors Yes-associated protein 1 (YAP) and transcriptional coactivator with PDZ binding motif (TAZ; reviewed in Seo and Kim, 2018). To gauge the impact of the bG/0 genotype on the Hippo pathway, we quantified YAP expression using quantitative Western blotting; no significant differences were observed (Figure 4H).

Finally, we quantified bG/0 MEF migration habits using a random cell migration assay (Figure 5, A–C). We observed that bG/0 MEFs migrated at rates similar to those in WT and bG/gG controls. No significant differences were observed for bG/0 directionality, direction autocorrelation, mean squared displacement (MSD), or speed from WT and bG/gG controls (Figure 5, D–G). These results lead us to conclude that the intact *Actg1* nucleotide sequence is not required for cell migration.

Loss of *Actg1* results in a unique myopathy

While β- and γ-actin are expressed in miniscule amounts in adult skeletal muscle compared with α-skeletal actin (Goldberg *et al.*, 1980; Hanft *et al.*, 2006), muscle-specific knockout of either *Actb* or *Actg1* results in a mild, but progressive age-dependent myopathy (Sonnemann *et al.*, 2006; Prins *et al.*, 2011). However, conversion of β-actin to γ-actin protein via gene editing had no effect on muscle function (Patrinostro *et al.*, 2018). bG/0 muscles were not different from WT or bG/gG controls in the percentage of centrally nucleated fibers (CNF), susceptibility to eccentric contraction induced force loss, muscle mass, fiber size, or fiber number (Figure 6, A and B; Supplemental Figure S3), but bG/0 muscles did present with significantly decreased specific isometric force (Figure 6C). bG/0 mice also displayed a hyperactivity phenotype in an open field assay (Supplemental Figure S4). Additionally, γ-actin protein expression in bG/0 muscle was not different from that in bG/gG (Figure 6D), suggesting that the myopathy is not due to hypomorphic γ-actin expression. Because these data suggest that bG/0 myopathy is not due to altered γ-actin levels, and because the myopathy differs from both *Actb* and *Actg1* conditional muscle-specific knockout models, we conclude that the novel skeletal muscle weakness of bG/0 is due to the loss of *Actg1* from a nonmuscle cell or tissue that supports skeletal muscle function, or loss of *Actg1* in the earliest stages of development.

Actg1 knockout does not exacerbate hearing phenotypes of *Actb*$^{c-g}$ mice

Based on studies in gene knockout and *Actb*$^{c-g}$ mice, both cytoplasmic actins have been shown to be important for maintenance of stereocilia in the inner ear with loss of either causing progressive hearing loss (Perrin *et al.*, 2010; Patrinostro *et al.*, 2018). To determine if the bG/0 genotype further compromises the structure or function of the inner ear, we employed scanning electron microscopy (SEM) and auditory brainstem response (ABR) testing in 6 wk-old and 16 wk-old WT, bG/gG, and bG/0 mice. Outer hair cell (OHC) stereocilia in 6 wk-old bG/0 mice had normal morphology. In

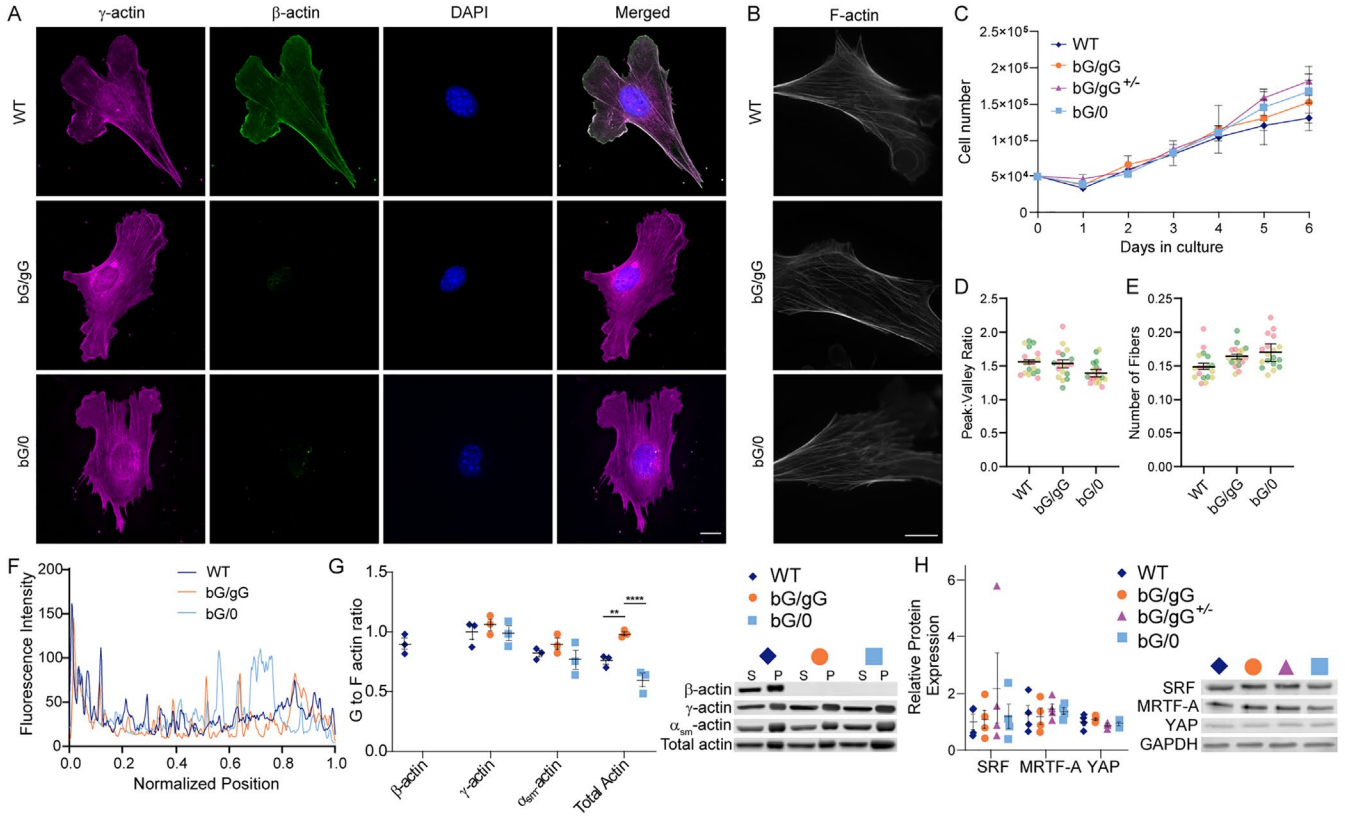

FIGURE 4: No growth or morphology phenotypes in bG/0 MEFs. (A) Representative images of WT, bG/gG, and bG/0 MEFs. γ-actin is labeled in magenta, β-actin is labeled in green, and nucleus is labeled in blue. Scale bar: 50 μm. (B) Representative images of phalloidin-stained actin filaments in WT, bG/gG, and bG/0 MEFs. Scale bar: 20 μm. (C) MEF growth curve of WT, bG/gG, bG/gG$^{+/-}$, and bG/0 embryos cultured for 6 d ($n = 4$). (D) Quantification of peak:valley ratios across linescans as a measure of stress fiber thickness and (E) relative number of fibers per cell ($N = 3$, $n = 6$). Each color represents an independent experiment. (F) Representative linescans of WT, bG/gG, and bG/0 MEFs. (G) Ratio of G- to F-actin for β-, γ-, α_{sm}-, and total actin in WT, bG/gG, and bG/0 MEFs ($n = 3$). (H) Relative expression of actin-associated proteins SRF, MRTF-A, and YAP normalized to GAPDH in WT, bG/gG, bG/gG$^{+/-}$, and bG/0 MEFs ($n = 4$). One- or two-way ANOVA with Bonferroni posttest was performed. For D and E, statistical analysis was performed on the means of independent experiments. Error bars are SEM. *$p < 0.05$, **$p < 0.01$, ***$p < 0.001$, ****$p < 0.0001$. Comparisons are not statistically significant unless otherwise indicated.

contrast, at 16 wk of age we observed variable lengths in OHC stereocilia rows 2 and 3 from both bG/gG, and bG/0 mice, which resembles the *Actb*$^{-/-}$, rather than the *Actg1*$^{-/-}$ phenotype. Additionally, some OHCs were lost in the base of cochlea (Figure 7, A and B). The ABR thresholds of bG/0 were not significantly different from those of bG/gG at either 6 or 16 wk of age, and both lines showed significant hearing loss at high frequencies compared with WT mice at 16 wk of age (Figure 7, C–D). This pattern of progressive high-frequency hearing loss is again consistent with that previously seen in hair cell-specific *Actb*$^{-/-}$ mice, but is different than that in *Actg1*$^{-/-}$ mice, which had progressive hearing loss at all sound frequencies. These data suggest that the *Actg1* nucleotide sequence is not necessary for auditory function because OHC structure and ABR thresholds were similar in bG/gG and bG/0 mice.

DISCUSSION

Previous data using various *Actb*$^{-/-}$ models suggested that loss of β-actin is lethal in mice, leading to the conclusion that β-actin is an essential cellular protein (Shawlot *et al.*, 1998; Shmerling *et al.*, 2005; Bunnell *et al.*, 2011). However, more recent studies utilizing CRISPR/Cas9 or TALENs generated a β-actin protein-specific knockout by editing the *Actb* nucleotide sequence to express γ-actin. These *Actb*$^{c-g}$ mice were overtly normal, demonstrating that it is not the β-actin protein that is essential for mouse development, but rather the intact *Actb* nucleotide sequence, suggesting that *Actb* has protein-independent function (Vedula *et al.*, 2017; Patrinostro *et al.*, 2018). An attempt was made to generate a mouse that expressed β-actin from *Actg1*, *Actg1*$^{c-b}$, but only three of the four amino acids were successfully edited. The partially edited *Actg1* mouse presented with no abnormal phenotypes, suggesting that the survival defect observed in *Actg1*$^{-/-}$ mice may also be due to loss of intact *Actg1* nucleotide sequence (Vedula *et al.*, 2017). Here we addressed whether expression of γ-actin exclusively from the edited *Actb*$^{c-g}$ allele could support mouse and cell viability. Most interestingly, our data revealed that the bG/0 mice present with significantly impaired survival, while expressing the same relative amount of γ-actin protein as the *Actb*$^{c-g}$ line with normal survival. Our data support an important protein-independent role for the *Actg1* nucleotide sequence.

Data collected here corroborate years of studies that emphasize that despite high sequence identity between β- and γ-actin, and their respective nucleotide sequences *Actb* and *Actg1*, the cytoplasmic actin genes and proteins have unique functions. Many of these studies have centered on genetically modified mice, and the

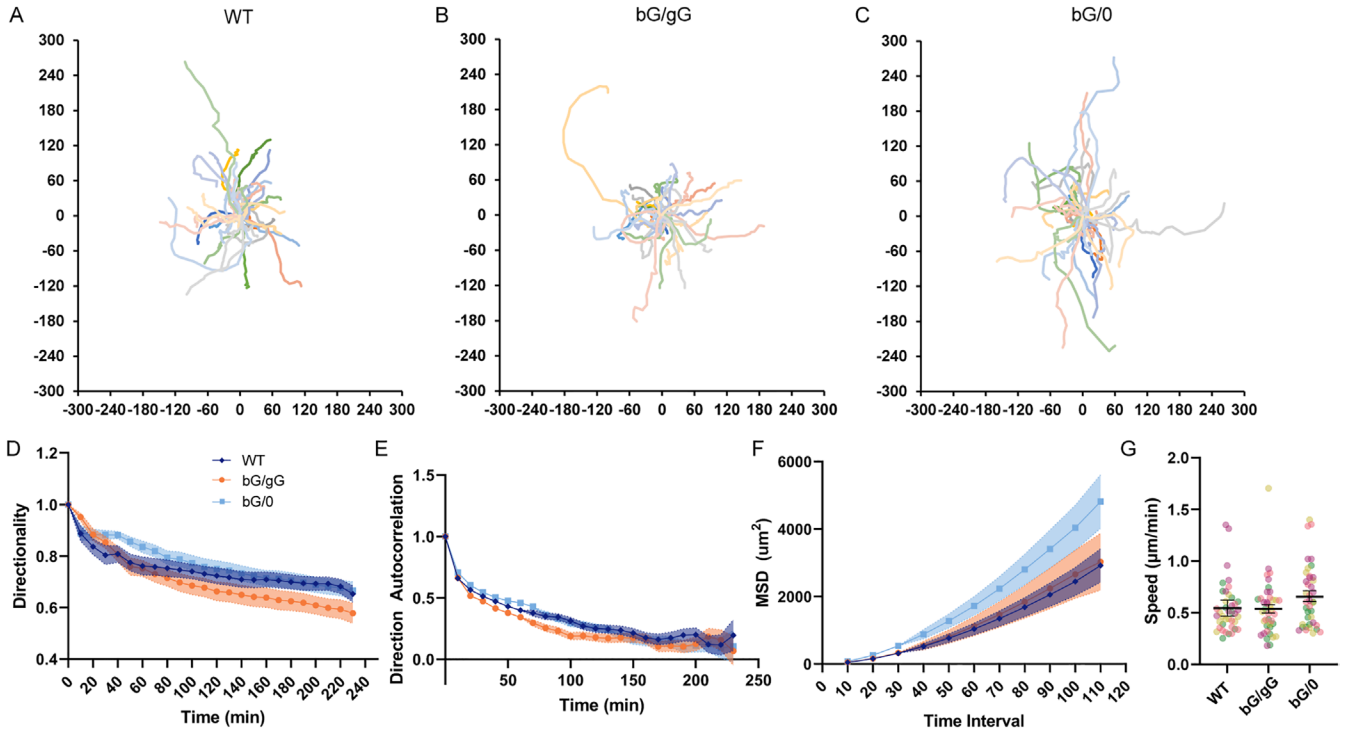

FIGURE 5: Normal cell motility in bG/0 MEFs. (A-C) Individual cell trajectories mapped from the origin for WT, bG/gG, and bG/0 MEFs for each genotype to characterize random migration patterns. Each different colored line indicates an individual cell path. (D) Directionality, (E) directional autocorrelation, (F) mean square displacement, and (G) speed; $N = 4$, $n = 10$ cells per embryo. For G, each color represents an independent experiment. For D-F, two-way ANOVA with repeated measures and Bonferroni posttest was performed. For G, one-way ANOVA with Bonferroni posttest was performed; statistical analysis was performed on the means of independent experiments. Error bars are SEM. Comparisons are not statistically significant unless otherwise indicated.

results of these various mouse models reveal that we cannot predict if an organismal function requires the cytoplasmic actin nucleotide sequence or protein, despite the high similarity of the two. While mouse survival is dependent on *Actb* (Bunnell *et al.*, 2011), we confirm here that it is also negatively impacted by loss of *Actg1*. Previous studies attributed the importance of γ-actin or *Actg1* for mouse lifespan and body mass to the protein (Belyantseva *et al.*, 2009; Bunnell & Ervasti, 2010), but here we demonstrate that the *Actg1* nucleotide sequence is required for normal mouse survival and growth. On the other hand, we have also identified protein-dependent functions for γ-actin that are not the same for β-actin. The *Actb* nucleotide sequence is required for cell proliferation (Bunnell & Ervasti, 2010; Patrinostro *et al.*, 2017), but here we showed that it is the loss of γ-actin protein that impairs proliferation in *Actg1*$^{-/-}$ MEFs rescued by reintroduction of γ-actin in the bG/0 mice (summarized in Table 1).

The phenotypic consequences of perturbing either a cytoplasmic actin gene or a protein were also observed through a novel skeletal muscle weakness phenotype in bG/0 mice. bG/0 muscle weakness was characterized by a significant decrease in specific isometric force measured without increases in the percentage of CNF, indicative of muscle necrosis and regeneration or increased susceptibility of force generation to eccentric contraction associated with muscle-specific ablation of *Actb* or *Actg1* (Sonnemann *et al.*, 2006; Prins *et al.*, 2011). Because γ-actin protein expression in bG/0 skeletal muscle was not different from that in bG/gG, which has normal muscle function, our data suggest that the skeletal muscle weakness novel to bG/0 may be due to the loss of *Actg1* and/or γ-actin from a nonmuscle cell or tissue that more indirectly impacts muscle strength. Alternatively, this discrepancy between models may arise from small differences in the knockout mechanism. The *Actg1*$^{-/-}$ knockout in bG/0 is constitutive and present in the earliest stages of embryogenesis (Belyantseva *et al.*, 2009), while muscle-specific *Actg1*$^{-/-}$ is a conditional knockout that is triggered by expression of Cre from the human α-skeletal actin (HSA) promotor, which only begins to express around 9 d post coitum (dpc; Miniou *et al.*, 1999). Therefore, if intact *Actg1* is required in the earliest stages of muscle development, the muscle-specific *Actg1*$^{-/-}$ mice may escape the myopathy observed in the bG/0 mice.

Exactly how the nucleotide sequences of the cytoplasmic actin genes confer their important functions remains elusive. Multiple lines of evidence identify functional noncoding regions of either gene. The importance of *Actb* may be due to local translation of the transcript via the *Actb* zipcode (Kislauskis *et al.*, 1994; Ross *et al.*, 1997; Artman *et al.*, 2014). Other regulatory elements have been identified in the *Actb* 3′ UTR and intron 3 of *Actg1* (DePonti-Zilli, Seiler-Tuyns, & Paterson, 1988; Lloyd & Gunning, 1993; Drummond & Friderici, 2013), suggesting these or other unidentified functional regions within noncoding sequences of either gene may serve *Actb* or *Actg1* nucleotide-dependent functions. While the aforementioned regions are largely involved in regulating expression of β- and γ-actin, other sequence elements could be involved in various cell functions through regulating expression of other genes. Microarray analysis of *Actb*$^{-/-}$ MEFs revealed dysregulation of genes involved in the cell cycle, actin dynamics, and myosin activity (Bunnell *et al.*, 2011); however, further characterization studies are needed to identify if *Actg1*$^{-/-}$ cells have similar expression changes and to clarify how either gene may be causing changes in gene expression.

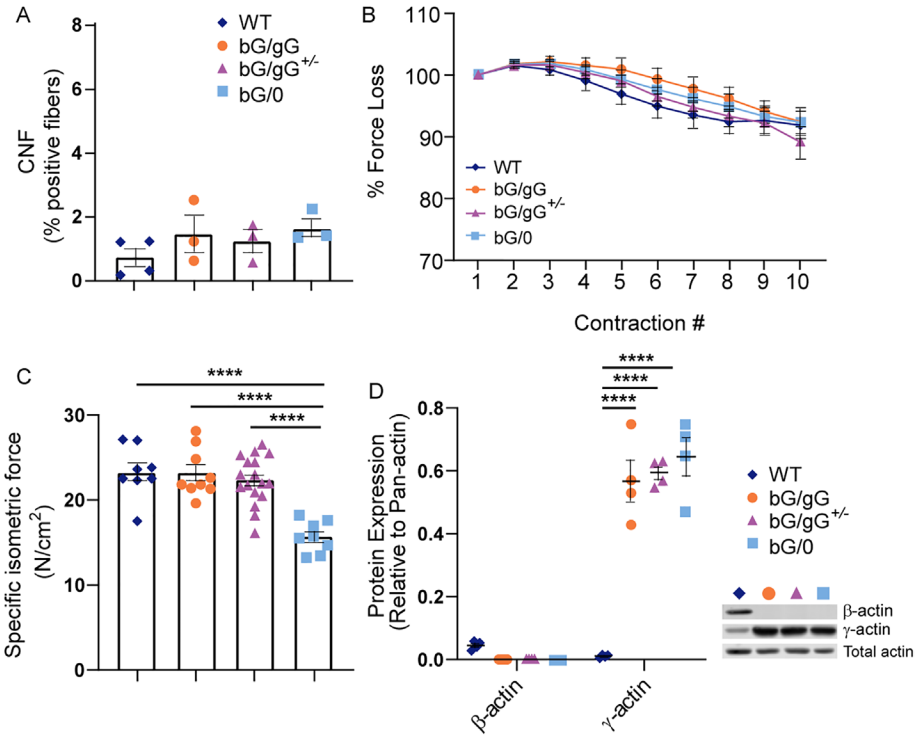

FIGURE 6: bG/0 mice exhibit skeletal muscle weakness in the absence of other myopathy phenotypes. (A) Percentage of fibers containing centrally nucleated fibers (CNF) of quadriceps muscle ($n \geq 3$). (B) Eccentric force loss (ECC) as a percentage of initial force in extensor digitorum longus (EDL) muscle and (C) specific isometric force in EDL muscle ($N \geq 4$, $n = 2$ muscles per mouse). (D) Relative expression of β-, γ-, and total actin of Dnase-enriched gastrocnemius muscle with representative Western blots of each, normalized to Pan-actin ($n = 4$). All experiments performed on WT, bG/gG, bG/gG$^{+/-}$, and bG/0 mice. One- or two-way ANOVA with Bonferroni posttest was performed. *$p < 0.05$, **$p < 0.01$, ***$p < 0.001$, ****$p < 0.0001$. Error bars are SEM. Comparisons are not statistically significant unless otherwise indicated.

In addition to demonstrating nucleotide-dependent functions for *Actg1* in mouse survival and skeletal muscle strength, we have also confirmed protein-dependent functions of cytoplasmic actins in hearing function and stereocilia structure in the inner ear. γ-Actin-specific functions might be revealed if the fully edited *Actg1*$^{c-b}$ mouse were generated. Vedula *et al.*, (2017) attempted to generate this γ-actin-specific knockout, but was only partially successful, so another attempt to complete this model would be beneficial in fully defining the differential roles of the cytoplasmic actin proteins. However, from a completely different perspective, we examined this same question with the bG/0 mice to uncover novel data identifying protein-independent functions of *Actg1*. Further investigation into the protein-independent functions of *Actb* and *Actg1* will be essential to determining how these nucleotide sequences are conferring important functions within an organism and likely reveal novel roles for noncoding DNA that may be relevant to other genes. Cytoplasmic β- and γ-actin have been highly evolutionarily conserved from birds to mammals, despite being 99% similar at the amino acid level and 89% identical at the nucleotide level (Perrin and Ervasti, 2010). Further clarification on the functional differences between the two will provide novel insights into the evolutionary significance of highly similar molecules that might be applied to other proteins and/or genes.

Another theory posits that differential translation rates resulting from the higher percentage of noncoding nucleotide differences between *Actb* and *Actg1* contribute to the importance of the cytoplasmic actin genes. It has been observed that γ-actin from *Actg1* is translated more slowly than β-actin from *Actb*, and these differential translation rates confer differences in focal adhesion turnover and cell migration (Zhang *et al.*, 2010; Vedula *et al.*, 2021).

Recent work by Vedula *et al.* (2021) found that exogenous expression of the γ-actin coding sequence flanked by the *Actb* promoter and 3′ untranslated sequence resulted in increased directional migration rates in immortalized MEFs, but had no effect on random cell migration rates, while expression of the β-actin coding sequence in the same context decreased migration rates. In this study, we found that exclusively expressing endogenous *Actb*-coded γ-actin in the bG/0 mice had no significant impact on random cell migration rates. We did not assess directional migration in bG/0 MEFs because previous work on *Actg1*$^{-/-}$ MEFs found that directional migration was unaffected by loss of the *Actg1* coding sequence and γ-actin protein (Bunnell and Ervasti, 2010). Discrepancies between these studies suggest that differences in the biological system may alter cytoplasmic actin function. Migration studies in *Actg1*$^{-/-}$ and bG/0 cells were conducted in primary cells with germline gene edits, while the study by Vedula *et al.* (2021) was conducted in immortalized cells expressing both exogenous and endogenous cytoplasmic actins.

MATERIALS AND METHODS

Request a protocol through *Bio-protocol*.

Mice

Animals were housed and treated in accordance with the standards set by the University of Minnesota Institutional Animal Care and Use Committee. All animal experiments were approved by the University of Minnesota Institutional Animal Care and Use Committee under protocol numbers 1806A36018 and 2106A39169. Mice were housed in a specific pathogen-free facility on a 12h light/dark cycle with ad libitum access to food and water. All mice used in this study were on the C57BL/6J background. *Actb*$^{c-g/c-g}$ (Patrinostro *et al.*, 2018) and *Actg1*$^{+/-}$ (Belyantseva *et al.*, 2009) mice were crossed and genotypes were determined as described previously (Patrinostro *et al.*, 2018; Sonnemann *et al.*, 2006). Mice were killed by cervical dislocation after anesthesia with Avertin at 3 mo of age for phenotypic analysis. Tissue was dissected and snap-frozen in liquid nitrogen.

Cell Culture

Primary WT, bG/gG, bG/gG$^{+/-}$, and bG/0 mouse embryonic fibroblasts (MEFs) were isolated from E13.5 embryos as described previously (Bunnell and Ervasti, 2010). MEFs were grown to approximately 80% confluency in MEF media (DMEM supplemented with 10% fetal bovine serum, 1% Pen/Strep, and 0.5 ug/mL Fungizone) and 1×10^6 cells were frozen at passage one in MEF freezing media

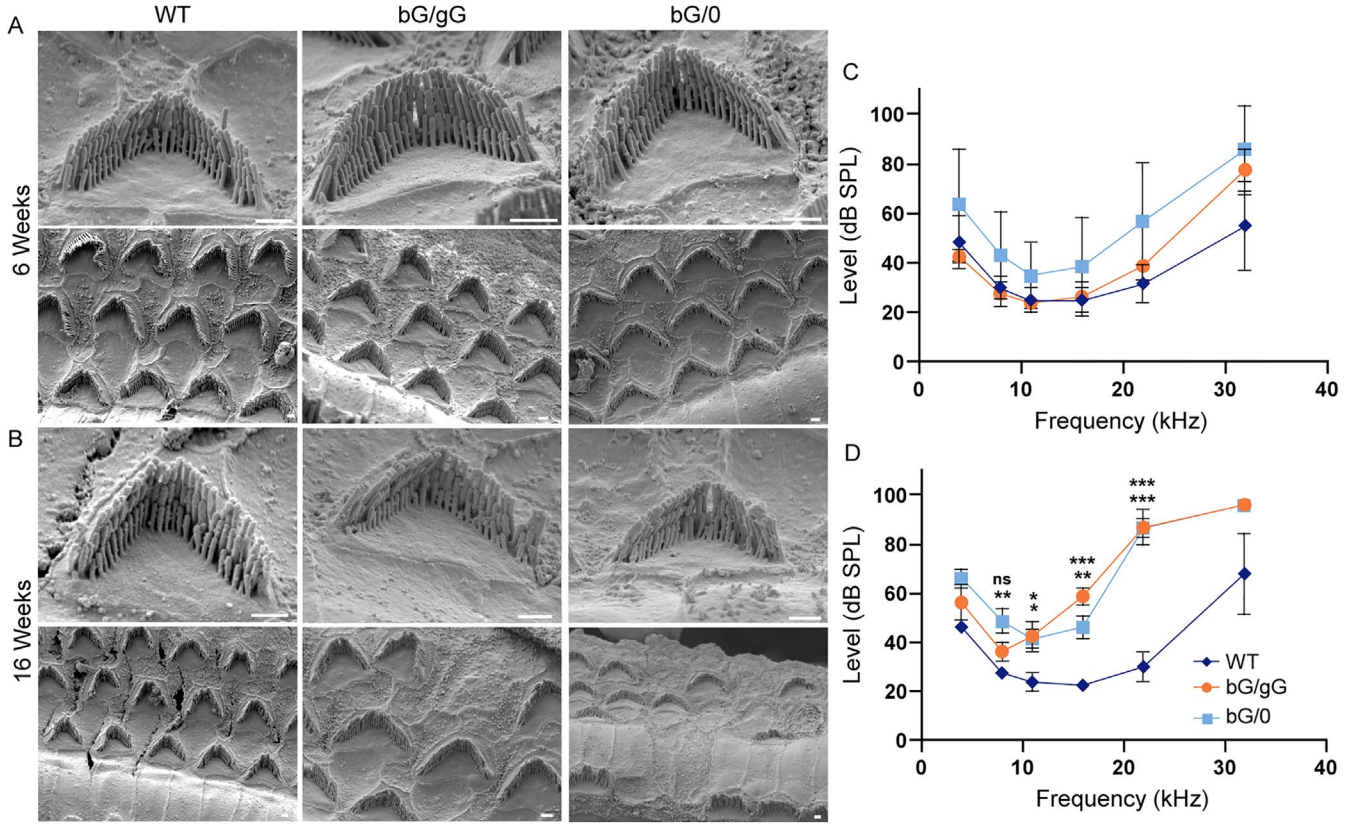

FIGURE 7: bG/0 mice have progressive hearing loss. (A, B) SEM images and (C, D) ABR of 6 wk- and 16 wk-old WT, bG/gG, and bG/0 mice (n ≥ 3). SEM images of cochlea middle turn OHC. Scale bar: 1 μm. ABR defined frequency in kilohertz is on the *x*-axis and threshold (in decibels) sound that elicits a response is on the *y*-axis. One-way ANOVA with Bonferroni posttest was performed. *$P < 0.05$, **$P < 0.01$, ***$P < 0.001$. Error bars are SD. For significance in D, Top symbols: bG/0 compared with WT; Bottom symbols: bG/gG compared with WT. Comparisons are not statistically significant unless indicated otherwise.

(95% fetal bovine serum + 5% DMSO). MEFs were then thawed and cultured in MEF media.

Mouse embryonic fibroblast proliferation assay

MEFs were seeded at a density of 5×10^4/well of a six-well plate, in duplicate, in MEF media and a single well of each plate was counted every day for 6 d using a hemocytometer.

Mouse embryonic fibroblast fixation, staining, and immunofluorescent imaging

Coverslips were coated in 5 μg/ml fibronectin, seeded with 2×10^4 MEFs, and incubated overnight in MEF media. The following day, cells were fixed with 4% paraformaldehyde in PBS for 30 min at room temperature (RT), washed 3 × 5 min with phosphate-buffered saline (PBS), permeablized for 10 min at RT with 0.1% Triton in PBS, and blocked for 30 min at RT with 3% bovine serum albumin (BSA) + 0.1% Triton in PBS. Coverslips were washed once with 0.1% Triton in PBS. For isoform-specific staining, coverslips were stained with the following primary antibodies in 3% BSA + 0.1% Triton in PBS overnight at 4°C: β-actin (1:400; Sigma-Aldrich, AC15) and γ-actin (affinity-purified γ-cyto actin rabbit 7577). For F-actin staining, coverslips were stained with Acti-Stain 555 phalloidin (cytoskeleton PHDH1-A) according to manufacturer's instructions. All coverslips were then washed 3 × 5min with PBS, rinsed with ddH_2O, and mounted with ProLong Gold Antifade with 4′,6-diamidino-2-phenylindole (DAPI) (Cell Signaling Technology 8961S). Images were collected using a 20×/NA0.75 or 60×/NA1.42 objective on a DeltaVision personalDV microscope with softWorx 7.2.1 (GE Technologies) using the same laser intensities and exposure times.

Function	*Actg1*	γ-actin
Mouse survival	+	–
Mouse growth	+	–
MEF proliferation	–	+
Skeletal muscle strength	+	–
Hearing	–	+
OHC stereocilia maintenance	–	+

Note: A "+" indicates that *Actg1* or γ-actin is involved in the corresponding function while a "-" indicates it is not involved.

TABLE 1: Functions dependent on the *Actg1* nucleotide sequence and γ-actin protein.

Image analysis

Images were analyzed using ImageJ (National Institutes of Health, Bethesda, MD, version 1.52p). Actin stress fiber thickness was quantified using fluorescence intensity of linescans across the widest portion of the cell body perpendicular to the fibers. The peaks and corresponding valleys were then determined, excluding the first and last peaks, which correspond to the edges of the cell. Fiber number totals were measured as the total number of peaks normalized to the width of the linescan. To quantify the proportion of peripheral

γ-actin, cells were masked and all background fluorescence was cleared. Cell masks were then outlined and dilated to define the cell periphery. From these measurements, the ratio of raw fluorescence intensity in the cell periphery to the raw fluorescence intensity of the internal area was then calculated. The cell masks were also used to measure circularity and aspect ratio.

Live cell imaging

A sample of 2×10^4 MEFs were cultured overnight in MEF media in a Nunc glass-bottomed dish (Thermo Scientific 150680). The following day, the MEF media was replaced with MEF media without phenol red + HEPES to stabilize the pH and the dishes were sealed with vacuum grease and a glass coverslip. Images were collected every 10 min for 4 h using a 10×/NA0.25 objective with phase contrast illumination on a DeltaVision personalDV in an environmental chamber maintained at 37°C. Cells were tracked using the Manual Tracking plugin for ImageJ (National Institutes of Health, Bethesda, MD, version 1.52 h) and the xy track data was analyzed using the DiPer plugin for Excel (Gorelik and Gautreau, 2014). Cells that divided or contacted other cells were excluded from analysis

qRT-PCR

WT and *Actb*$^{c-g}$ mouse isoactin controls were generated and respective primer sets were verified previously to be isoform-specific (Patrinostro *et al.*, 2017, 2018). For whole tissue, samples were pulverized using liquid nitrogen and a mortar and pestle and homogenized in Trizol using a 27G needle and syringe. Total RNA was extracted from homogenized tissue and MEF samples using the Bio-Rad Aurum Total RNA Mini-Kit (7326820) according to manufacturer's instructions. RNA concentration was measured using a NanoDrop 1000 spectrophotometer (ThermoFisher Scientific). A Bio-Rad iScript Advanced cDNA synthesis kit (1725037) was used to synthesize first-strand cDNA from a standard amount of RNA. Isoactin and *Actb*$^{c-g}$ control samples were used in a series of 10-fold dilutions to generate standard curves, and MEF or tissue cDNA samples were amplified in parallel using Bio-Rad SsoAdvanced Universal SYBR Green Supermix (1725270) and isoform-specific primers using the Bio-Rad CFX96 Real Time System C1000 touch thermal cycler. Transcript quantities were calculated in picomoles using the standard curves.

Western blotting

Brain, lungs, and gastrocnemius muscles were pulverized in liquid nitrogen using a mortar and pestle. MEF, brain, and lung protein was extracted in 1% SDS buffer in 1X PBS with a cocktail of protease inhibitors (100 µM aprotinin, 0.79 mg/ml benzamide, 1 µM calpain, 1 µM calpeptin, 10 µM E-64, 10 µM leupeptin, 0.1 mg/ml pepstatin, 1 mM phenylmethylsulfonyl fluoride) and MEF lysates were sonicated (Model 150V/T ultrasonic homogenizer; BioLogics). All samples were then boiled and centrifuged to remove the insoluble fraction. Pulverized gastrocnemius muscle was subjected to low-salt extraction and DNase enrichment as described previously (Hanft *et al.*, 2006). Equal amounts of cleared lysates (25 µg brain or lung, 20 µg gastrocnemius, and 15 µg MEF) were separated by SDS-polyacrylamide gel electrophoresis (SDS-PAGE) before being transferred to a PVDF membrane and blocked for 30 min in 5% nonfat milk in PBS. The following antibodies were used: β-actin (1:5,000; Sigma-Aldrich, AC15), γ-actin (1:5,000 mAB 2-4), α_{sm}-actin (1:5,000; Sigma-Aldrich, 1A4), Pan-actin (1:5,000; Seven Hills Bioreagents, C4), SRF (1:1,000; Santa Cruz Biotechnology, G-20), MRTF-A (1:1,000; Cell Signaling Technology, E2V2I), or YAP (1:500, Abnova) with glyceraldehyde 3-phosphate dehydrogenase (GAPDH; 1:5,000; Sigma-Aldrich, G9545) as a loading control and secondary antibodies DyLight 800 anti-mouse IgG (1:10,000; Cell Signaling Technology, 5257S) and DyLight 680 anti-rabbit IgG (1:10,000; Cell Signaling Technology, 5366S). Blots were imaged using the Odyssey CLx infrared scanner (LI-COR Biosciences) and protein bands were quantified using LI-COR Image Studio Software.

G- to F-actin ratio

Equal numbers of WT, bG/gG, and bG/0 MEFs were pelleted before the experiment. G- and F-actin fractions were isolated from MEFs using the G-actin/F-actin in vivo assay kit (Cytoskeleton, #BK037) according to manufacturer's instructions and Western blotted for β-actin, γ-actin, α_{sm}-actin, and total actin (see *Western Blotting* for a complete list of antibodies). Blots were imaged using the Odyssey CLx Infrared scanner (LI-COR Biosciences) and fluorescence intensities of G- and F-actin protein bands were quantified using LI-COR Image Studio Software to determine the ratio of G- to F-actin for each genotype.

Open field activity assay

Mice were placed in an open-field apparatus for 15 min and total horizontal distance and vertical movement counts were measured based on infrared beam breaks. Activity was measured using the AccuScan system (Columbus Instruments).

Muscle immunofluorescence imaging

Quadriceps muscles from each mouse line were cryopreserved in melting isopentane for 30 s and 7-µm transverse cryosections were obtained (Leica CM3050 S). For immunofluorescence, sections were fixed in acetone at -20°C for 15 min and subsequently washed three times in PBS before being blocked in 5% goat serum for 30 mins at RT. Sections were incubated for >1 h in primary antibody (rat monoclonal anti-Laminin 1:500; Sigma, L06631) at RT. Slides were then washed three times in PBS before incubation with Alexa Fluor 488 goat anti-rat IgG (1:1000; ThermoFisher, A-11006) secondary for 30 mins at RT. Sections were finally washed three times in PBS and mounted in ProLong Gold Antifade with 4′,6- diamidino-2-phenylindole (DAPI) to visualize nuclei (ThermoFisher Scientific). Images were acquired on a Leica DM5500 B microscope equipped with a Leica HC PLAN APO 10× objective and stitched together with LASX software (Leica) to allow visualization of the entire quadriceps. SMASH—semi-automatic muscle analysis using segmentation of histology software—was used to analyze and quantify centrally located nuclei, fiber number, and fiber size (Smith and Barton, 2014).

Ex vivo EDL force measurements

Contractile function of EDL muscles was assessed according to methods described previously (Moran *et al.*, 2005). Mice were anesthetized with sodium pentobarbital (75-100 mg/kg body mass). EDL muscles were dissected and mounted on a 300B-LR dual-mode muscle lever system (Aurora Scientific) with 5-0 suture in a 1.2-ml bath assembly with oxygenated (95:5% O_2/CO_2) Krebs Ringer bicarbonate (Krebs) buffer maintained at 25°C. The stimulator and muscle lever system were controlled by computer using a KPCI-3108 interface board (Keithley Instruments) and TestPoint software (SuperLogics). Muscles were adjusted to their anatomical optimal length (L_o) based on resting tension, with length being measured from the distal myotendonous junction to the proximal myotendonous junction using digital calipers. Before eccentric contractions were performed, maximal isometric tetanic force (P_o) was measured every 2 min by stimulating the muscle to contract for 200 ms at 175

Hz until force plateaued. A series of 10 eccentric contractions (ECC) were performed and the peak force of each contraction was recorded. For each ECC force measurement, the muscle was passively shortened to 95% L_o and then stimulated for 200 ms while the muscle was simultaneously lengthened to 105% L_o at a velocity of 0.5 L_o/s. Each eccentric contraction was separated from the next eccentric contraction by 3 min of rest to prevent fatigue (Lowe *et al.*, 1994). The force measured at each eccentric contraction was expressed as a percentage of the force produced during the first contraction.

Auditory brainstem response

Auditory brainstem response (ABR) waveforms for mice were collected using a Tucker Davis Technologies System 3 at frequencies of 4, 8, 11, 16, 22, and 32 kHz as described previously (Patrinostro *et al.*, 2018). Scalp potentials were recorded using subdermal electrodes following anesthetization with Avertin. Waveforms for each frequency were collected starting at 90 dB, decreasing in 5-dB steps to a subthreshold level. The collected waveforms were stacked and the lowest level of stimulation that resulted in a definite waveform was considered to be the threshold.

Scanning electron microscopy

Dissected cochlea were fixed in 2.5% glutaraldehyde, 0.1 M sodium cacodylate, 2 mM $CaCl_2$ overnight at 4°C and then decalcified in 170 mM EDTA in PBS for 16 h at 4°C. Dissected organ of Corti was incubated in 2% each of arginine, glutamine, glycine, and sucrose in water overnight at RT, followed by incubation in 2% tannic acid and guanidine hydrochloride for 2 h at RT and 1% OsO_4 in water for 1 h at RT, with extensive water washes between steps. The samples were transitioned to 100% ethanol, critical point dried from CO_2 and sputter coating with gold. Samples were imaged using a JEOL JSM-7800F field emission scanning electron microscope.

Statistics

All statistics were calculated using GraphPad Prism Software (version 9.0.2). One- or two-way ANOVAs with Bonferroni posttest were performed based on the specific data set and significance was determined with $*p < 0.05$, $**p < 0.01$, $***p < 0.001$, and $****p < 0.0001$.

ACKNOWLEDGMENTS

This work was supported by NIH Grant T32-AG029796 to L.J.S., R01-AR049899 to J.M.E., and R01-DC015495 to B.J.P.

REFERENCES

Artman L, Dormoy-Raclet V, von Roretz C, Gallouzi IE (2014). Planning your every move: the role of β-actin and its post-transcriptional regulation in cell motility. Sem Cell Dev Biol, 34, 33–43.

Baarlink C, Wang H, Grosse R (2013). Nuclear actin network assembly by formins regulates the SRF coactivator MAL. Science, 340, 864–867.

Belyantseva IA, Perrin BJ, Sonnemann KJ, Zhu M, Stepanyan R, McGee J, Frolenkov G, Walsh E, Friderici K, Friedman T, Ervasti JM (2009). γ-Actin is required for cytoskeletal maintenance but not development. Proc Natl Acad Sci USA, 106, 9703–9708.

Bunnell TM, Burbach BJ, Shimizu Y, Ervasti JM (2011). β-Actin specifically controls cell growth, migration, and the G-actin pool. Mol Biol Cell, 22, 4047–4058.

Bunnell TM, Ervasti JM (2010). Delayed embryonic development and impaired cell growth and survival in Actg1 null mice. Cytoskeleton, 67, 564–572.

Chen A, Arora PD, McCulloch CA, Wilde A (2017). Cytokinesis requires localized β-actin filament production by an actin isoform specific nucleator. Nat Commun, 8, 1–11.

Davis J, Molkentin JD (2014). Myofibroblasts: trust your heart and let fate decide. J Mol Cell Cardiol, 70, 9–18.

DePonti-Zilli L, Seiler-Tuyns A, Paterson BM (1988). A 40-base-pair sequence in the 3′ end of the beta-actin gene regulates beta-actin mRNA transcription during myogenesis. Proc Natl Acad Sci USA, 85, 1389–1393.

Drazic A, Timmerman E, Kajan U, Marie M, Varland S, Impens F, Gevaert K, Arnesen T (2021). The final maturation state of β-actin involves N-terminal acetylation by NAA80 not N-terminal arginylation by ATE1. J Mol Biol 167397.

Drummond MC, Friderici KH (2013). A Novel Actin mRNA Splice Variant Regulates ACTG1 Expression. PLOS Genet 9, e1003743.

Dugina V, Zwaenepoel I, Gabbiani G, Clément S, Chaponnier C (2009). Beta and gamma-cytoplasmic actins display distinct distribution and functional diversity. J Cell Sci 122(Pt 16), 2980–2988.

Esnault C, Stewart A, Gualdrini F, East P, Horswell S, Matthews N, Treisman R (2014). Rho-actin signaling to the MRTF coactivators dominates the immediate transcriptional response to serum in fibroblasts. Genes Dev 28, 943–958.

Goldberg DJ, Harris DA, Lubit BW, Schwartz JH (1980). Analysis of the mechanism of fast axonal transport by intracellular injection of potentially inhibitory macromolecules: evidence for a possible role of actin filaments. Proc Natl Acad Sci USA 77, 7448–7452.

Gorelik R, Gautreau A (2014). Quantitative and unbiased analysis of directional persistence in cell migration. Nat Protocols 9, 1931–1943.

Hanft LM, Rybakova IN, Patel JR, Rafael-Fortney JA, Ervasti JM (2006). Cytoplasmic γ-actin contributes to a compensatory remodeling response in dystrophin-deficient muscle. Proc Natl Acad Sci USA 103, 5385–5390.

Hinz B (2007). Formation and function of the myofibroblast during tissue repair. J Invest Dermatol 127, 526–537.

Hüttelmaier S, Zenklusen D, Lederer M, Dictenberg J, Lorenz M, Meng XH, Bassell GJ, Condeelis J, Singer RH (2005). Spatial regulation of β-actin translation by Src-dependent phosphorylation of ZBP1. Nature 438, 512–515.

Karakozova M, Kozak M, Wong CCL, Bailey AO, Yates JR, Mogilner A, Zebroski H, Kashina A (2006). Arginylation of β-actin regulates actin cytoskeleton and cell motility. Science 313, 192–196.

Kashina AS (2006). Differential arginylation of actin isoforms: the mystery of the actin N-terminus. Trends Cell Biol 16, 610–615.

Kashina AS (2020). Regulation of actin isoforms in cellular and developmental processes. Sem Cell Dev Biol 102, 113–121.

Kislauskis EH, Zhu X, Singer RH (1994). Sequences responsible for intracellular localization of beta-actin messenger RNA also affect cell phenotype. J Cell Biol, 127, 441–451.

Latham SL, Ehmke N, Reinke PYA, Taft MH, Eicke D, Reindl T, Stenzel W, Lyons M, Friez M, Lee J, *et al.* (2018). Variants in exons 5 and 6 of ACTB cause syndromic thrombocytopenia. Nat Commun 9, 4250. https://doi.org/10.1038/s41467-018-06713-0

Lloyd C, Gunning P (1993). Noncoding regions of the gamma-actin gene influence the impact of the gene on myoblast morphology. J Cell Biol 121, 73–82.

Lowe DA, Warren GL, Hayes DA, Farmer MA, Armstrong RB (1994). Eccentric contraction-induced injury of mouse soleus muscle: effect of varying $[Ca^{2+}]o$. J Appl Physiol 76, 1445–1453.

Miniou P, Tiziano D, Frugier T, Roblot N, Le Meur M, Melki J (1999). Gene targeting restricted to mouse striated muscle lineage. Nucleic Acids Res 27, e27–e30.

Miyajima H, Moteki H, Day T, Nishio SYA, Murata T, Ikezono T, Takeda H, Abe S, Iwasaki S, Takahashi M, *et al.* (2020). Novel ACTG1 mutations in patients identified by massively parallel DNA sequencing cause progressive hearing loss. Sci Rep 10, 1–10.

Moran AL, Warren GL, Lowe DA (2005). Soleus and EDL muscle contractility across the lifespan of female C57BL/6 mice. Exp Gerontol 40, 966–975.

Müller M, Diensthuber RP, Chizhov I, Claus P, Heissler SM, Preller M, Taft M, Manstein DJ (2013). Distinct functional interactions between actin isoforms and nonsarcomeric myosins. PLOS ONE 8, e70636.

Olson EN, Nordheim A (2010). Linking actin dynamics and gene transcription to drive cellular motile functions. Nat Rev Mol Cell Biol 11, 353–365.

Otey CA, Kalnoski MH, Bulinski JC (1988). Immunolocalization of muscle and nonmuscle isoforms of actin in myogenic cells and adult skeletal muscle. Cell Motil Cytoskeleton 9, 337–348.

Otey CA, Kalnoski MH, Lessard JL, Bulinski JC (1986). Immunolocalization of the gamma isoform of nonmuscle actin in cultured cells. J Cell Biol 102, 1726–1737.

Pan F, Hüttelmaier S, Singer RH, Gu W (2007). ZBP2 facilitates binding of ZBP1 to beta-actin mRNA during transcription. Mol Cell Biol 27, 8340–8351.

Pathan-Chhatbar S, Taft MH, Reindl T, Hundt N, Latham SL, Manstein DJ (2018). Three mammalian tropomyosin isoforms have different regulatory effects on nonmuscle myosin-2B and filamentous β-actin in vitro. J Biol Chem 293, 863–875.
Patrinostro X, O'Rourke AR, Chamberlain CM, Moriarity BS, Perrin BJ, Ervasti JM (2017). Relative importance of βcyto-and γcyto-actin in primary mouse embryonic fibroblasts. Mol Biol Cell 28, 771–782.
Patrinostro X, Roy P, Lindsay A, Chamberlain CM, Sundby LJ, Starker CG, Ervasti JM, Perrin BJ (2018). Essential nucleotide- and protein-dependent functions of Actb/β-actin. Proc Natl Acad Sci USA 115, 7973–7978. https://doi.org/10.1073/pnas.1807895115
Pavlyk I, Leu NA, Vedula P, Kurosaka S, Kashina A (2018). Rapid and dynamic arginylation of the leading edge β-actin is required for cell migration. Traffic 19, 263–272.
Perrin BJ, Ervasti JM (2010). The actin gene family: function follows isoform. Cytoskeleton 67, 630.
Perrin BJ, Sonnemann KJ, Ervasti JM (2010). β-Actin and γ-actin are each dispensable for auditory hair cell development but required for stereocilia maintenance. PLoS Genet 6, e1001158.
Pollard TD, Cooper JA (2009). Actin, a central player in cell shape and movement. Science 326, 1208–1212.
Prins KW, Call JA, Lowe DA, Ervasti JM (2011). Quadriceps myopathy caused by skeletal muscle-specific ablation of βcyto-actin. J Cell Sci 124, 951–957.
Rivière JB, Van Bon BWM, Hoischen A, Kholmanskikh SS, O'Roak BJ, Gilissen C, Gijsen S, Sullivan C, Christian S, Abdul-Rahman O, *et al*. (2012). De novo mutations in the actin genes ACTB and ACTG1 cause Baraitser-Winter syndrome. Nat Genet 44, 440–444.
Ross AF, Oleynikov Y, Kislauskis EH, Taneja KL, Singer RH (1997). Characterization of a beta-actin mRNA zipcode-binding protein. Mol Cell Biol 17, 2158–2165.
Rubenstein PA, Wen KK (2014). Insights into the effects of disease-causing mutations in human actins. Cytoskeleton 71, 211–229.
Saha S, Mundia MM, Zhang F, Demers RW, Korobova F, Svitkina T, Perieteanu A, Dawson J, Kashina A (2010). Arginylation regulates intracellular actin polymer level by modulating actin properties and binding of capping and severing proteins. Mol Biol Cell 21, 1350–1361.
Seo J, Kim J (2018). Regulation of Hippo signaling by actin remodeling. BMB Rep 51, 151.
Shawlot W, Deng JM, Fohn LE, Behringer RR (1998). Restricted β- galactosidase expression of a hygromycin-lacZ gene targeted to the β- actin locus and embryonic lethality of β-actin mutant mice. Transgen Res 7, 95–103.
Shmerling D, Danzer CP, Mao X, Boisclair J, Haffner M, Lemaistre M, Schuler V, Kaeslin E, Korn R, Bürki K, *et al*. (2005). Strong and ubiquitous expression of transgenes targeted into the -actin locus by Cre/lox cassette replacement. Genesis 42, 229–235.
Shuster CB, Lin AY, Nayak R, Herman IM (1996). βCAP73: A novel β actin-specific binding protein. Cell Motil Cytoskeleton 35, 175–187.
Smith LR, Barton ER (2014). SMASH - semi-automatic muscle analysis using segmentation of histology: A MATLAB application. Skel Muscle 4, 1–16.
Sonnemann KJ, Fitzsimons DP, Patel JR, Liu Y, Schneider MFF, Moss RL, Ervasti JMM (2006). Cytoplasmic γ-actin is not required for skeletal muscle development but its absence leads to a progressive myopathy. Dev Cell 11, 387–397.
Tomasek JJ, Gabbiani G, Hinz B, Chaponnier C, Brown RA (2002). Myofibroblasts and mechano-regulation of connective tissue remodelling. Nat Rev Mol Cell Biol 3, 349–363.
Vartiainen MK, Guettler S, Larijani B, Treisman R (2007). Nuclear actin regulates dynamic subcellular localization and activity of the SRF cofactor MAL. Science 316, 1749–1752.
Vedula P, Kurosaka S, Leu NA, Wolf YI, Shabalina SA, Wang J, Sterling S, Dong D, Kashina A (2017). Diverse functions of homologous actin isoforms are defined by their nucleotide, rather than their amino acid sequence. eLife 6. https://doi.org/10.7554/eLife.31661
Vedula P, Kurosaka S, Mactaggart B, Ni Q, Papoian GA, Jiang Y, Dong D, Kashina A (2021). Different translation dynamics of β-and γ-actin regulates cell migration. ELife 10. https://doi.org/10.7554/ELIFE.68712
Welch AY, Riley KN, D'Souza-Schorey C, Herman IM (2005). Arf6 modulates the beta-actin specific capping protein, betacap73. Methods Enzymol 404, 377–387.
Zhang F, Saha S, Shabalina SA, Kashina A (2010). Differential arginylation of actin isoforms is regulated by coding sequence-dependent degradation. Science 329, 1534–1537.
Zhu M, Yang T, Wei S, DeWan AT, Morell RJ, Elfenbein JL, Fisher R, Leal S, Smith R, Friderici KH (2003). Mutations in the γ-actin gGene (ACTG1) are associated with dominant progressive deafness (DFNA20/26). Am J Human Genet 73, 1082–1091.